

Ultrafast dynamics of bright and dark excitons in monolayer WSe₂ and heterobilayer WSe₂/MoS₂

Jan Philipp Bange,¹ Paul Werner,¹ David Schmitt,¹ Wiebke Bennecke,¹ Giuseppe Meneghini,²
AbdulAziz AlMutairi,³ Marco Merboldt,¹ Kenji Watanabe,⁴ Takashi Taniguchi,⁵ Sabine
Steil,¹ Daniel Steil,¹ R. Thomas Weitz,^{1,6} Stephan Hofmann,³ G. S. Matthijs Jansen,¹
Samuel Brem,² Ermin Malic,² Marcel Reutzler,^{1,*} and Stefan Mathias^{1,6,†}

¹*I. Physikalisches Institut, Georg-August-Universität Göttingen,
Friedrich-Hund-Platz 1, 37077 Göttingen, Germany*

²*Fachbereich Physik, Philipps-Universität, 35032 Marburg, Germany*

³*Department of Engineering, University of Cambridge, Cambridge CB3 0FA, U.K.*

⁴*Research Center for Electronic and Optical Materials,
National Institute for Materials Science,
1-1 Namiki, Tsukuba 305-0044, Japan*

⁵*Research Center for Materials Nanoarchitectonics,
National Institute for Materials Science,
1-1 Namiki, Tsukuba 305-0044, Japan*

⁶*International Center for Advanced Studies of Energy Conversion (ICASEC),
University of Göttingen, Göttingen, Germany*

Abstract

The energy landscape of optical excitations in mono- and few-layer transition metal dichalcogenides (TMDs) is dominated by optically bright and dark excitons. These excitons can be fully localized within a single TMD layer, or the electron- and the hole-component of the exciton can be charge-separated over multiple TMD layers. Such intra- or interlayer excitons have been characterized in detail using all-optical spectroscopies, and, more recently, photoemission spectroscopy. In addition, there are so-called hybrid excitons whose electron- and/or hole-component are delocalized over two or more TMD layers, and therefore provide a promising pathway to mediate charge-transfer processes across the TMD interface. Hence, an in-situ characterization of their energy landscape and dynamics is of vital interest. In this work, using femtosecond momentum microscopy combined with many-particle modeling, we quantitatively compare the dynamics of momentum-indirect intralayer excitons in monolayer WSe_2 with the dynamics of momentum-indirect hybrid excitons in heterobilayer $\text{WSe}_2/\text{MoS}_2$, and draw three key conclusions: First, we find that the energy of hybrid excitons is reduced when compared to excitons with pure intralayer character. Second, we show that the momentum-indirect intralayer and hybrid excitons are formed via exciton-phonon scattering from optically excited bright excitons. And third, we demonstrate that the efficiency for phonon absorption and emission processes in the mono- and the heterobilayer is strongly dependent on the energy alignment of the intralayer and hybrid excitons with respect to the optically excited bright exciton. Overall, our work provides microscopic insights into exciton dynamics in TMD mono- and bilayers.

* marcel.reutzel@phys.uni-goettingen.de

† smathias@uni-goettingen.de

I. INTRODUCTION

Exfoliated and artificially stacked monolayers of transition metal dichalcogenides (TMDs) have been shown to be a highly tuneable material platform for exploring optical excitations and correlated interactions on the atomic scale [1–7]. After first experiments identified the transition from an indirect to a direct semiconductor when exfoliating bulk TMDs to the monolayer limit [8, 9], subsequent studies characterized the strong exciton response to an optical excitation [10–13]. Importantly, these pioneering all-optical experiments are for the most part only sensitive to radiative recombination processes within the light-cone [14, 15]. However, in addition to these bright excitons, it is meanwhile well-known that also tightly bound dark excitons contribute to the energy landscape of excitons [16–21]. For example, for momentum-indirect dark excitons in a monolayer TMD, the exciton’s electron and hole component can reside in different valleys of the TMD Brillouin zone (figure 1(c, e)). In the case that TMD homo- and heterostructures are assembled by more than one layer, the situation can become even more complex: The twist-angle between two neighbouring TMD layers can be varied from 0° to 60° , and, in this way, the high-symmetry points of the Brillouin zones are offset in momentum space. Hence, so-called interlayer excitons for which the electron- and the hole-component are charge-separated across the interface are typically momentum-indirect and thus optically dark (figure 1(d, f)) [22].

First direct access to these dark excitons has been provided in optical-pump-midinfrared-probe experiments [23, 24]. With the development of high-repetition rate extreme ultraviolet light sources [25–28], time- and angle-resolved photoelectron spectroscopy (trARPES) [29, 30] has become applicable to probe the energetics and dynamics of bright and dark excitons. First experiments focused onto the ultrafast exciton and charge carrier dynamics in semiconducting bulk [31–35] and wafer-scale [36–40] TMDs. More recently, empowered by the development of time-of-flight momentum microscopes [41, 42], trARPES has been successfully applied to probe the formation dynamics of momentum-indirect intralayer excitons [43, 44] and the valley depolarization dynamics [45] in exfoliated monolayer TMDs. In addition, the cascaded exciton transition from bright intralayer to dark interlayer excitons has been quantified in an artificially stacked TMD heterobilayer [46, 47].

These seminal trARPES experiments of exfoliated TMDs all focus on excitons that are either of full intra- or interlayer character: The exciton’s electron and hole either reside both in a single TMD layer, or are charge-separated between both layers. Until today, no trARPES experiment

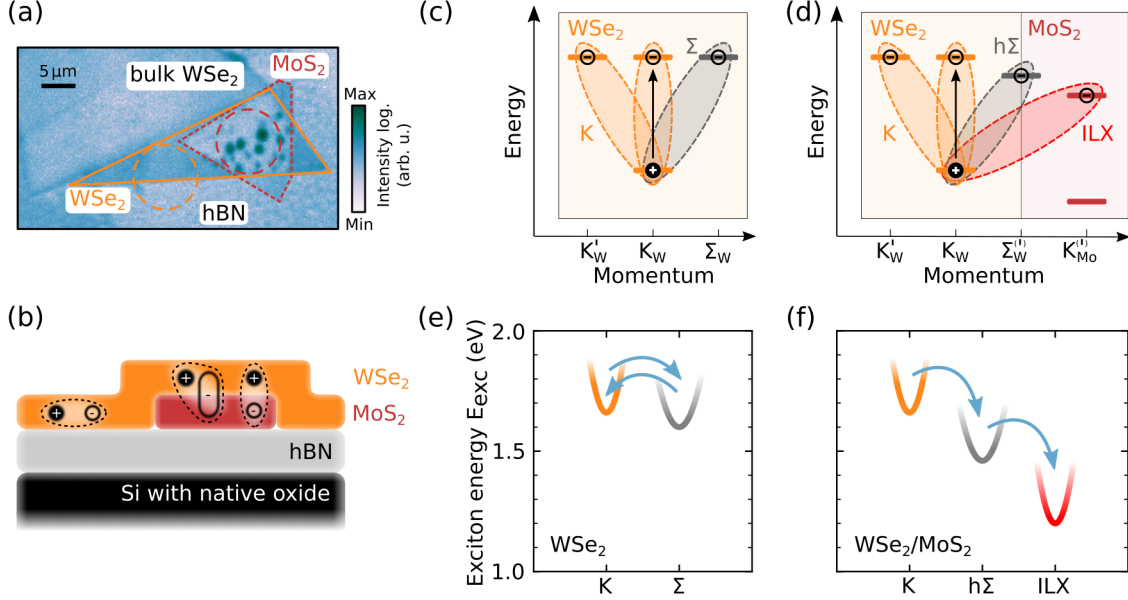


FIG. 1. Real-space sample structure and energy landscape of monolayer WSe_2 and heterobilayer $\text{WSe}_2/\text{MoS}_2$. (a) Real-space resolved photoemission image of the monolayers WSe_2 (orange polygon) and MoS_2 (dark red dashed polygon). Femtosecond momentum microscopy experiments of the monolayer WSe_2 and the heterobilayer $\text{WSe}_2/\text{MoS}_2$ are performed in the regions-of-interest indicated by the orange and dark red circles, respectively. (b) Schematic sketch of the TMD heterostructure after excitation with a 1.7 eV light pulse. Intralayer excitons are formed in the WSe_2 monolayer and the $\text{WSe}_2/\text{MoS}_2$ heterobilayer. In the $\text{WSe}_2/\text{MoS}_2$ heterostructure, the energetically most stable state is the interlayer exciton where the electron and the hole component are localized in the WSe_2 and the MoS_2 layer, respectively. In addition, hybrid excitons are formed for which the exciton's hole is fully localized in the WSe_2 layer and the exciton's electron has probability density in the WSe_2 and the MoS_2 layer. (c,d) Single-particle energy landscape of monolayer WSe_2 and heterobilayer $\text{WSe}_2/\text{MoS}_2$. The filled bars indicate the single-particle valence and conduction band extrema at the Brillouin zone's high-symmetry points. The ovals indicate the Coulomb correlation between the single-particle electrons and holes, and the letters label the electron-hole pairs, as introduced in the main text. (e,f) Energy landscape of excitons in the WSe_2 monolayer and the $\text{WSe}_2/\text{MoS}_2$ heterobilayer. The energies E_{exc} are obtained in experiment, and the blue arrows indicate the dominant scattering pathways.

has focused on the case where hybridization between the neighbouring TMD layers leads to the formation of a new type of exciton where either the electron-, the hole-, or the electron- and the hole-component are delocalized between both layers (figures 1(b)). Importantly, these so-called

hybrid excitons are of great interest due to their potential to mediate charge transfer across a TMD interface [34, 46, 48–52]. Moreover, they have a high oscillator strength and a sensitivity to external electrical fields due to their partial intra- and interlayer character [20, 53–59].

In this article, we study the impact of interlayer hybridization on the energy landscape of excitons and the resulting femto- to picosecond dynamics. In a joint theory-experiment effort, we directly compare the layer-localized Σ exciton in monolayer WSe₂ with the hybrid $h\Sigma$ exciton in heterobilayer WSe₂/MoS₂ (figure 1(c-f)). For both excitons, the hole-component to the exciton is fully layer-localized and found in the K_W valley valence band maximum (VBM) of WSe₂. In contrast, the exciton’s electron, which resides in the Σ valley of the conduction band, is either fully layer localized (WSe₂) or has a significant degree of interlayer hybridization (WSe₂/MoS₂). First, we experimentally quantify the bright and dark exciton energies E_{exc}^i of the correlated two-particle energy landscape. Second, we identify exciton-phonon scattering as the dominating mechanism for the formation of intralayer Σ and hybrid $h\Sigma$ excitons. And third, we show that the sub-ps exciton thermalization dynamics are significantly affected by the energy alignment of the Σ and $h\Sigma$ exciton with respect to the optically excited exciton.

II. BRIGHT AND DARK EXCITONS IN WSE₂ AND WSE₂/MOS₂

The major goal of this manuscript is the identification of hybrid excitons in the trARPES experiment and the evaluation of their impact on the exciton relaxation dynamics. Therefore, we describe the low energy landscape of excitons as calculated by solving the Wannier equation [6, 20, 21, 49, 60, 61]. All relevant excitations are summarized in the energy diagrams in figure 1(c-f).

If the monolayer WSe₂ is pumped with 1.7 eV photons, bright A1s excitons of WSe₂ are resonantly excited (black arrow in figure 1(c)). We label this exciton as K as its electron and hole component reside in the K_W valley conduction band minimum (CBM) and VBM, respectively. Note that throughout the manuscript, we do not differentiate between K excitons that are bound at K_W or K'_W valleys, because we cannot distinguish them in experiment. In addition to the bright A1s exciton, two distinct momentum-indirect dark excitons can be formed in a subsequent scattering process: On the one hand, there are momentum-indirect dark excitons for which the electron- and the hole-component are found in the Σ_W and the K_W valleys, respectively; these excitons are labelled as Σ throughout our work (figure 1(c, e)). On the other hand, momentum-indirect excitons

for which the electron- and the hole-component are momentum-offset and found in the K_W or K'_W valleys can be formed. Importantly, while it is expected that these momentum-indirect excitons are energetically favorable over the optically excited bright excitons [21, 57, 58], where the electron- and the hole-component are bound in the same K_W or K'_W valley, within the energy resolution of the photoemission experiment, it is not possible to separate these excitons. Hence, we label both of them with K throughout the manuscript.

In the WSe_2/MoS_2 heterostructure, 1.7 eV photons can be used to resonantly excite the A1s exciton in WSe_2 (black arrow in figure 1(d)). A similar resonance frequency for the optical excitation of WSe_2 A1s excitons in the mono- and the heterobilayer region can be rationalized based on the fact that wavefunction hybridization at the K_W valleys is negligible [48, 51, 60, 62, 63]. In addition, because the optical excitation of A1s excitons of monolayer MoS_2 would require at least 1.9 eV light-pulses [47, 50, 63, 64], the MoS_2 monolayer is not directly excited. The optically excited WSe_2 A1s excitons can decay to form momentum-indirect excitons, where the electron- and the hole-component are momentum-offset between the K_W and K'_W valleys. Because we cannot differentiate between these momentum-indirect excitons and the bright A1s excitons in the photoemission experiment, as in the case of the WSe_2 monolayer, we label both these bright and momentum-indirect excitons with K. More interestingly for our study, momentum-indirect hybrid $h\Sigma$ excitons are formed for which the exciton's hole and electron can be found in the K_W and the $\Sigma^{(l)}$ valley, respectively: Here, the $\Sigma^{(l)}$ valley conduction bands of the WSe_2 and MoS_2 are hybridized, and, in consequence, the $h\Sigma$ exciton can be described in the hybrid exciton basis with approximately 30% intra- and 70% interlayer character [46]. Note that the hybrid character of this exciton's electron component is indicated by the letter 'h' in the abbreviation. With this hybrid character of the $h\Sigma$ excitons, interlayer charge transfer is strongly favored and interlayer excitons (ILX) can be formed [46, 49]. For ILX, because of the negligible hybridization of the wavefunctions at the WSe_2 $K_W^{(l)}$ and MoS_2 $K_{Mo}^{(l)}$ valleys, the exciton's electron and hole component are again fully localized in the monolayers (figure 1(d)).

III. MOMENTUM MICROSCOPY: ENERGY LANDSCAPE OF EXCITONS

In this section, we experimentally quantify the exciton energies of the bright and dark excitons in the WSe_2 monolayer and the WSe_2/MoS_2 heterolayer. All energies are summarized in table I.

A. Femtosecond momentum microscopy of exfoliated TMDs

In order to establish the most direct experimental comparison of the exciton energy landscape of the WSe₂ monolayer and the twisted WSe₂/MoS₂ heterobilayer, we fabricate a single sample that contains distinct areas in which the monolayer WSe₂ flake and the WSe₂/MoS₂ heterostructure are found (figure 1(a)). We have chosen a doped silicon wafer with a native oxide layer as the substrate for the heterostructure, because it ensures high quality trARPES data that is not affected by sample charging (figure 1(b)). Moreover, the TMD flakes are stacked on 20-30 nm hexagonal boron nitride [65] for best interface quality [66]. Before the trARPES experiments, the sample is annealed for 1 h to 670 K. In the real-space-resolved photoemission electron microscopy image in figure 1(a), the boundaries of the WSe₂ and MoS₂ monolayers are traced by orange and dark red (dashed) polygons, respectively. The twist-angle of the heterostructure is quantified to $9.8\pm 0.8^\circ$ [46].

Time-resolved photoemission spectroscopy of exfoliated mono- and heterobilayers becomes possible by using our setup for femtosecond momentum microscopy (cf. refs. [25, 67, 68]). We resonantly excite the bright A_{1s} exciton of WSe₂ with 1.7 eV 40 fs light pulses (*s*-polarized). Photoemission from the occupied band structure and the excitons is induced with time-delayed 26.5 eV 20 fs light pulses (*p*-polarized) that are created in a table-top 500 kHz repetition rate high-harmonic generation beamline [25, 69, 70]. For each delay between the pump and the probe laser pulse, the time-of-flight momentum microscope (ToF-MM, Surface Concept GmbH) collects three-dimensional data cubes that contain information on the two in-plane momenta k_x and k_y and the energy E of the detected photoelectrons [25, 42]. Notably, by inserting an aperture into the real-space plane of the microscope, the experiment is sensitive to the exciton dynamics in a sample region with a diameter of 10 μm (orange and red circles in figure 1(a)) [43–46].

The momentum microscopy experiment can be used to directly characterize and compare the occupied band structure of monolayer WSe₂ and heterobilayer WSe₂/MoS₂ (figure 2). In both sample areas, the spin-split valence bands at the WSe₂ K_W valley can be identified (labelled (1) and (2) in the magenta energy-distribution-curves (EDCs)). In the heterobilayer, in addition, the MoS₂ valence band is observed at $E-E_{\text{VBM}} = 0.94 \pm 0.05$ eV (labelled (3) in figure 2(b)). While the dispersion of the WSe₂ valence bands are similar at the K_W valleys of the mono- and the heterobilayer, it is strikingly different at the Γ valley: In the monolayer, only a single band at the Γ valley is observed (horizontal arrow, figure 2(a)). In contrast, in the heterobilayer, we find two

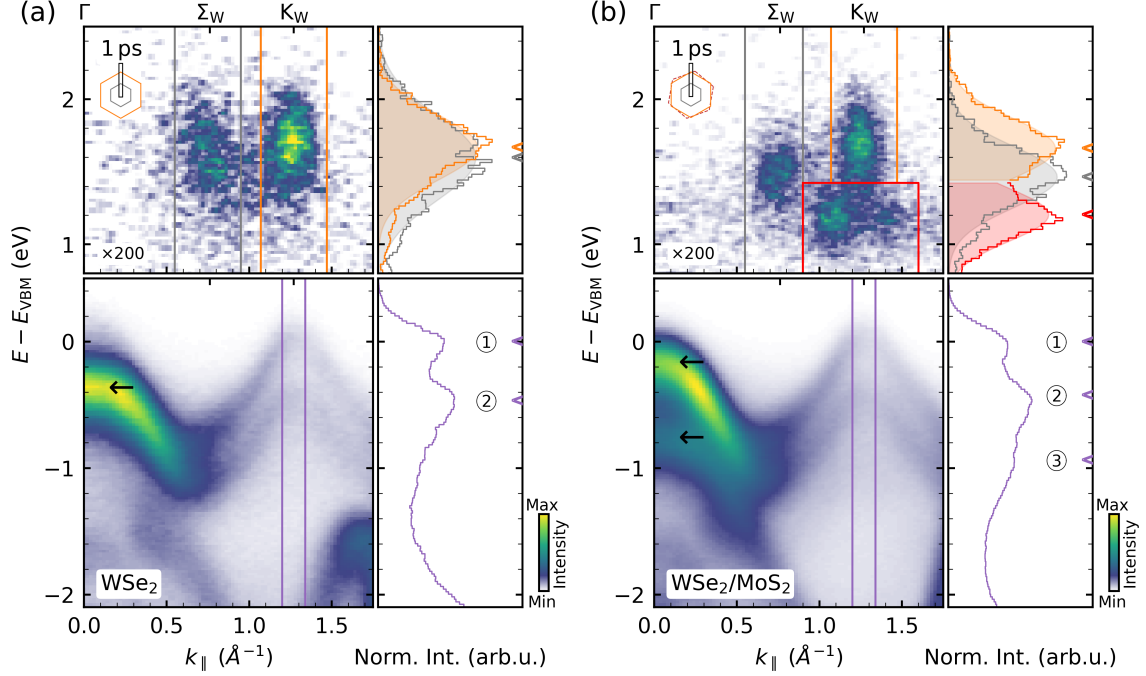


FIG. 2. Energy- and momentum-resolved photoemission spectra of monolayer WSe_2 and heterobilayer $\text{WSe}_2/\text{MoS}_2$ along the Γ - K_W direction (inset). (a) The occupied valence band structure of monolayer WSe_2 is dominated by a single-band at the Γ valley (black horizontal arrow) and the spin-split valence bands at the K_W valley (labelled (1) and (2) in the EDC). At a pump-probe delay of 1 ps and a photoemission energy of ≈ 1.7 eV, exciton photoemission yield from intralayer K (orange) and Σ (grey) excitons is detected. (b) The occupied valence band structure of heterobilayer $\text{WSe}_2/\text{MoS}_2$ is characterized by the WSe_2 spin-split valence bands at the K_W valley (labelled (1) and (2) in the EDCs) and the valence band of MoS_2 (3), for which the spin-splitting is not resolved. At the Γ valley, interlayer hybridization leads to the formation of two bands (horizontal black arrows). At a pump-probe delay of 1 ps, exciton photoemission yield is detected from the intralayer K excitons (orange), hybrid $h\Sigma$ excitons (grey) and ILX (red). The photoemission energy from hybrid $h\Sigma$ exciton's is significantly reduced when compared to the intralayer K (monolayer and heterobilayer) and Σ (monolayer) excitons. The energy-momentum cuts are obtained by summation of all six measured Γ - K_W (Γ - K'_W) directions.

energetically separated bands that are a clear indication for interlayer hybridization (two horizontal arrows in figure 2(b)) [71–73].

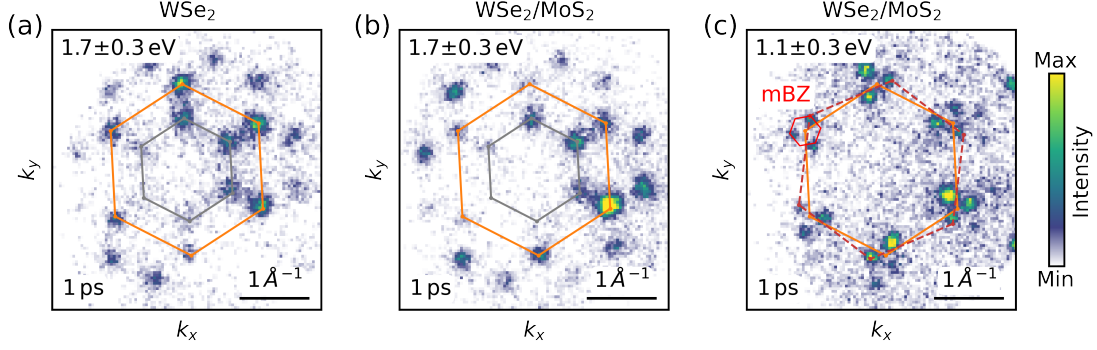


FIG. 3. Momentum-resolved photoemission maps at the energies of the intralayer, hybrid and interlayer excitons in monolayer WSe_2 and heterobilayer $\text{WSe}_2/\text{MoS}_2$. The pump-probe delay and the photoemission energy with respect to the WSe_2 VBM are given in the figure. All momentum maps are integrated in an energy window ± 0.3 eV around the center energy. (a) In the WSe_2 monolayer, the exciton photoemission momentum fingerprints of intralayer K (orange) and Σ (grey) show spectral weight at the $\text{K}_\text{W}^{(\prime)}$ and $\Sigma_\text{W}^{(\prime)}$ valleys of the WSe_2 hexagonal Brillouin zone. (b) In the $\text{WSe}_2/\text{MoS}_2$ heterobilayer, exciton photoemission from the intralayer K (orange) and the hybrid $h\Sigma$ (grey) excitons is found at the $\text{K}_\text{W}^{(\prime)}$ and $\Sigma_\text{W}^{(\prime)}$ valleys of the WSe_2 hexagonal Brillouin zones. (c) The momentum-misalignment of the Brillouin zones of WSe_2 (orange hexagon) and MoS_2 (dark red dashed hexagon) leads to a complex photoemission signature from ILX that can be described within the moiré mini Brillouin zone (mBZ, red hexagon).

B. Spectroscopy of excitons in monolayer WSe_2 and heterobilayer $\text{WSe}_2/\text{MoS}_2$

Having identified these distinct spectroscopic signatures of the electronic band structure that allow the direct discrimination of the mono- and the heterobilayer region in the trARPES experiment, in the next step, we probe the energetics of the optical excitations of the WSe_2 monolayer. Therefore, optical pump pulses with a center energy of 1.7 eV are used in order to be resonant to the WSe_2 A1s exciton (fluence: $280 \mu\text{J}/\text{cm}^{-2}$, exciton density: 5.4×10^{12} excitons/ cm^{-2}). We find spectral weight above the valence bands that we attribute to photoelectrons being emitted from excitons (figure 2(a)). Specifically, at a pump-probe delay of 1 ps, photoemission yield is detected at the K_W and the Σ_W valleys of the WSe_2 Brillouin zone (orange and grey hexagon in figure (3a), respectively). These spectral signatures can be attributed to photoemission from intralayer K and Σ excitons, consistent with earlier reports [43, 44].

When applying similar excitation conditions to the $\text{WSe}_2/\text{MoS}_2$ heterobilayer region, much richer spectral signatures are detected in the momentum microscopy experiment: A complex dis-

tribution of photoemission intensity is detected above the WSe₂ valence bands in an energy window ranging from 0.9 eV to 1.9 eV (figure 2(b), 1 ps pump-probe delay). The momentum-map centered at an energy of 1.7 eV above the WSe₂ VBM shows spectral weight at the momenta of the K_W and the Σ_W valleys that we attribute to photoemission signal from intralayer K and hybrid hΣ excitons (figure 3(b), orange and grey hexagon, respectively). At a lower energy (figure 3(c), E-E_{VBM} ≈ 1.1 eV), we find a complex momentum structure of the photoemission intensity that can be attributed to ILX: Spectral weight is detected at the K_{M0} valley and the additional κ valleys that are described within the moiré mini Brillouin zone (mBz, red hexagon). This hallmark of the moiré superlattice imprinted onto the exciton photoemission signature from the interlayer ILX excitons is discussed in detail in ref. [46].

C. Energy landscape of excitons in WSe₂ and WSe₂/MoS₂

Having identified the major photoemission spectral signatures of excitons, we aim to experimentally quantify the energy landscape of bright and dark excitons in the mono- and the hetero-bilayer sample. For this, first, we have to discuss at which energy the photoemission experiment detects single-particle photoelectrons that have initially been bound in the correlated exciton state. In the process of photoemission from an exciton, the Coulomb correlation between the exciton’s electron and hole is broken at the cost of the exciton binding energy. As described by Weinelt *et al.* [74] and others [35, 47, 75–81], the single-particle photoelectron from an exciton will be detected one exciton energy E_{exc}^i above the energy of the single-particle band where the former hole contribution to the exciton remains in the sample, i.e., at

$$E_{\text{elec}} = E_{\text{hole}} + E_{\text{exc}}^i + \hbar\omega \quad (1)$$

with E_{hole} and E_{elec} as the single-particle energy of hole and the electron-state, respectively; furthermore with E_{exc}^i as the exciton energy and $\hbar\omega$ as the probe photon energy. Importantly, Eq. 1 sets the energy of the WSe₂ VBM at the K_W valley as the natural reference point of the present experiment, because the single-particle hole of all probed excitons remains in this valley once photoemission has occurred (cf. figure 1(c,d)).

Hence, we can quantify the exciton energy E_{exc}^i of all contributing intralayer, hybrid and interlayer excitons by analysing the EDCs taken at the K_W, the Σ_W and the K_{M0} (κ) valleys (figure 2). Following Eq. 1, we then calculate the energy difference between each exciton photoemission

TABLE I. Summary of the experimentally quantified exciton energies E_{exc}^i in monolayer WSe₂ and heterobilayer WSe₂/MoS₂.

	monolayer WSe ₂	heterobilayer WSe ₂ /MoS ₂
$E_{\text{exc}}^{\text{K}}$ (eV)	1.67 ± 0.05	1.66 ± 0.05
E_{exc}^{Σ} (eV)	1.60 ± 0.05	-
$E_{\text{exc}}^{\text{h}\Sigma}$ (eV)	-	1.46 ± 0.05
$E_{\text{exc}}^{\text{ILX}}$ (eV)	-	1.20 ± 0.05

signal and the energy of the K_{W} valley VBM. All exciton energies E_{exc}^i quantified for the WSe₂ mono- and the WSe₂/MoS₂ heterobilayer are summarized in table I.

Having experimentally measured the exciton energies E_{exc}^i , we are now in the position to systematically compare those values. First, we find that, within the experimental error, the intralayer K exciton energy is comparable in the mono- and the heterobilayer region (1.67 ± 0.05 eV vs. 1.66 ± 0.05 eV). For WSe₂/MoS₂, this result strongly supports the expectation that excitons, where the electron- and hole-component are localized in the K_{W} valleys, are not affected by interlayer hybridization [48, 51, 60]. In contrast, we find that the hybrid character of the $\text{h}\Sigma$ excitons indeed leads to a renormalization of the exciton energy: The interlayer hybridization leads to a reduction of the exciton energy from 1.60 ± 0.05 eV (Σ exciton, monolayer WSe₂) to 1.46 ± 0.05 eV ($\text{h}\Sigma$ exciton, heterobilayer WSe₂/MoS₂). This observation is a direct experimental verification of seminal photoluminescence experiments that reported a changed emission energy for hybrid excitons, if the degree of hybridization is controlled, e.g., by the twist angle [51, 82–84].

IV. ULTRAFAST EXCITON DYNAMICS IN WSE₂ AND WSE₂/MOS₂

Having characterized the energy landscape of excitons, we now turn to the exciton scattering dynamics. Specifically, the goal of the analysis is to pinpoint the impact of the intralayer Σ and hybrid $\text{h}\Sigma$ excitons on the relaxation dynamics. Therefore, first, we compare the experimentally measured exciton dynamics with microscopic many-particle calculations that allow us to identify exciton-phonon scattering as the dominant mechanism for intervalley thermalization and the formation of the intralayer Σ and hybrid $\text{h}\Sigma$ excitons. Second, we focus on the sub-ps dynamics in

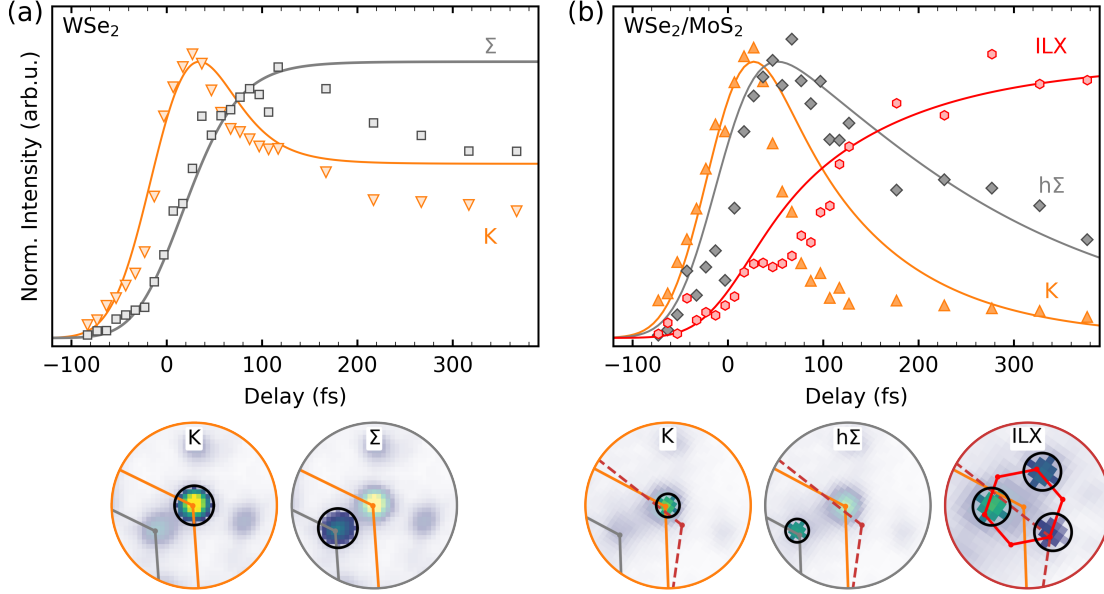


FIG. 4. Direct comparison of the ultrafast exciton dynamics in (a) monolayer WSe_2 and (b) heterobilayer $\text{WSe}_2/\text{MoS}_2$. The symbols show the pump-probe delay-dependent photoemission yield from excitons, and the solid lines are based on microscopic calculations. The exciton photoemission yield is filtered in the black-circled regions-of-interest indicated in the momentum-maps.

order to elucidate the impact of the different exciton energies of the intralayer Σ and the hybrid $h\Sigma$ exciton on the exciton relaxation cascade.

A. Exciton-phonon scattering: Formation of intralayer Σ and hybrid $h\Sigma$ excitons

The femtosecond momentum microscopy experiment provides direct access to the ultrafast dynamics of bright and dark excitons. The symbols in the main panels of figure 4 show the pump-probe delay-dependent photoemission yield from the intralayer K (orange), intralayer Σ (grey), hybrid $h\Sigma$ (grey) and ILX (red) excitons. In addition, the femtosecond evolution of exciton occupation as calculated in our microscopic model is plotted as solid lines of the respective color.

In the WSe_2 monolayer (figure 4(a)), photoemission yield from the K exciton peaks at pump-probe delays close to 40 fs. Delayed to this process, we find that spectral weight from momentum-indirect Σ excitons (grey) increases on a 100 fs timescale. This rise of the photoemission yield from the intralayer Σ excitons is in agreement with momentum microscopy experiments by Madéo *et al.* [43] and Wallauer *et al.* [44]. Moreover, the rise time is also in agreement with our micro-

TABLE II. Summary of the experimentally quantified rise and decay times of photoemission yield from excitons.

	monolayer WSe ₂	heterobilayer WSe ₂ /MoS ₂
$\tau_{\text{fast}}^{\text{K}}$ (fs)	70±10	28±2
$\tau_{\text{slow}}^{\text{K}}$ (fs)	1500±200	1900±800
$\tau_{\text{WSe}_2}^{\Sigma}$ (fs)	1050±60	-
$\tau_{\text{WSe}_2/\text{MoS}_2, \text{fast}}^{\text{h}\Sigma}$ (fs)	-	110±40
$\tau_{\text{WSe}_2/\text{MoS}_2, \text{slow}}^{\text{h}\Sigma}$ (fs)	-	1600±800
$\tau_{\text{rise}}^{\Sigma}$ (fs)	36±3	-
$\tau_{\text{rise}}^{\text{h}\Sigma}$ (fs)	-	34±3
$\tau_{\text{rise}}^{\text{ILX}}$ (fs)	-	120±20

scopic calculations that include exciton-light and exciton-phonon interaction. From the model, we therefore identify exciton-phonon scattering as the dominant mechanism for the formation of intralayer Σ excitons. Note that for pump-probe delays >100 fs, the exciton occupation calculated in the model overestimates the experimentally measured photoemission intensity from both excitons. The reason for this deviation is that the model does not include decay processes and thus overestimates the exciton occupation for longer pump-probe delays.

The pump-probe delay-dependent photoemission yield from excitons measured in the WSe₂/MoS₂ heterobilayer is shown in figure 4(b). We find a direct hierarchy in the onset of rising photoemission yield from the three types of excitons, i.e., the K excitons (orange), the hybrid h Σ excitons (grey), and the ILX (red). Again, the dynamics is in excellent agreement with our microscopic calculations, such that we can identify exciton-phonon scattering as the dominant mechanism for the formation of hybrid h Σ excitons.

B. Monolayer WSe₂: Steady state of phonon emission and absorption processes

So far, we have found that the intervalley relaxation processes in monolayer WSe₂ and heterobilayer WSe₂/MoS₂ are phonon-mediated and lead to the formation of intralayer Σ and hybrid h Σ excitons, respectively. However, even though the intervalley relaxation proceeds via the same

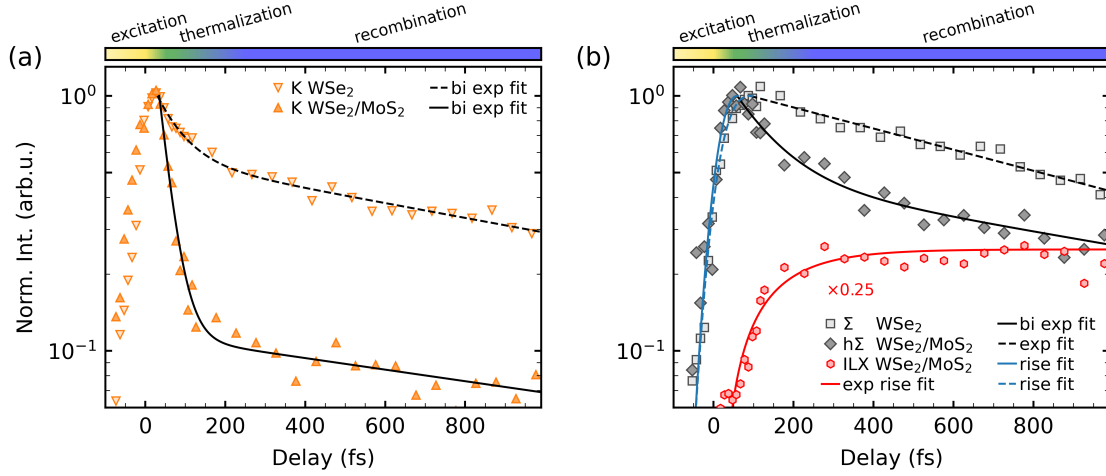


FIG. 5. Quantitative analysis of the intralayer and hybrid exciton dynamics. In the yellow, green and blue shaded delay regions, excitons are optically excited, thermalize and radiatively recombine, respectively. (a) Pump-probe-delay evolution of photoemission signal from K excitons in monolayer WSe₂ (empty triangles) and heterobilayer WSe₂/MoS₂ (filled triangles); the dashed and solid lines are bi-exponential decay fits to the data. (b) Quantitative evaluation of the formation and relaxation dynamics of intralayer Σ excitons (empty squares, grey) and hybrid $h\Sigma$ excitons (filled squares, grey). The rise time of the excitons is evaluated with a one-level rate equation model (blue dashed and solid line, respectively). The decay dynamics is approximated by bi- and single-exponential fits, respectively. The rise time of the ILX (red circles) is fitted with a single exponential function (red line). All rise and decay constants are summarized in table II.

mechanism, we find distinctly different decay dynamics of the contributing intralayer and hybrid excitons on the sub-ps timescale (figure 5 and table II). In the following, we pinpoint the origin of the different dynamics to the relative energy alignment of the intralayer Σ and hybrid $h\Sigma$ excitons with respect to the intralayer K excitons, which has direct impact on the efficiency of exciton-phonon scattering processes.

In monolayer WSe₂, the energy difference between the optically excited K and the intralayer Σ exciton is $\Delta E_{\text{exc}}^{\text{WSe}_2} = E_{\text{exc}}^{\text{K}} - E_{\text{exc}}^{\Sigma} = 0.07 \pm 0.10$ eV. Hence, phonon emission and absorption processes with typical energies of 0.03 eV [85] can efficiently create a steady state between both excitonic species, i.e., $\text{K} \rightleftharpoons \Sigma$, where the relative exciton occupation is given by degenerate Bose-Einstein distributions [21]. In order to identify this steady state in the photoemission data, we plot the sub-ps pump-probe delay-dependent photoemission intensity from K and Σ excitons on a logarithmic intensity axis in figure 5(a) and 5(b), respectively. As indicated by the yellow, green

and blue marked areas, the sub-ps dynamics of K excitons can be divided into overall three characteristic timescales. On the sub-40-fs timescale (yellow, figure 5(a)), photoemission yield from K excitons increases due to the optical excitation. For increasing pump-probe delay, the decaying photoemission intensity can be approximated by a bi-exponential function. Here, the two decay times $\tau_{\text{WSe}_2, \text{fast}}^{\text{K}} = 70 \pm 10$ fs and $\tau_{\text{WSe}_2, \text{slow}}^{\text{K}} = 1.5 \pm 0.2$ ps describe the fast and the slow component of the dynamics that are dominant in the green and blue delay-regions, respectively. In direct comparison to time-resolved all-optical spectroscopies, the slow component $\tau_{\text{WSe}_2, \text{slow}}^{\text{K}}$ can be attributed to radiative recombination processes of the bright excitons [50, 63, 86]. However, the interpretation of the fast time constant $\tau_{\text{WSe}_2, \text{fast}}^{\text{K}}$ is more complex (green): First, it contains information on the decay of the coherent exciton polarization towards the incoherent K exciton population [44, 87], which is not the focus of our study. Second, and more importantly, $\tau_{\text{WSe}_2, \text{fast}}^{\text{K}}$ is dominant in the delay-window that is necessary to establish a steady state between phonon absorption and emission events transferring K into Σ excitons and vice versa. In agreement with this assignment, we find that photoemission intensity from momentum-indirect Σ excitons, which are formed due to the decay of K excitons, rises on the same timescale and peaks at 100 fs (yellow and green delay-region in figure 5(b)). For longer delays (blue delay-region), the Σ exciton photoemission intensity decays and is described by a single-exponential fit with a decay time of $\tau_{\text{WSe}_2}^{\Sigma} = 1.1 \pm 0.1$ ps. Notably, it has already been suggested that the decay of momentum-indirect Σ excitons dominantly proceeds via phonon absorption processes that first transfer the Σ excitons into bright K excitons that can, subsequently, decay in a radiative process [15, 21, 88]. Our analysis verifies this proposition, because the experimentally quantified decay time $\tau_{\text{WSe}_2}^{\Sigma}$ of dark Σ excitons is in reasonable agreement with the radiative decay time $\tau_{\text{WSe}_2, \text{fast}}^{\text{K}}$ of K excitons (cf. table II).

C. Heterobilayer WSe₂/MoS₂: Phonon emission processes and formation of interlayer excitons

The situation is significantly different for the WSe₂/MoS₂ heterobilayer. The hybrid character of the h Σ exciton leads to a reduction of its exciton energy and thus to an energy difference of $\Delta E_{\text{exc}}^{\text{WSe}_2/\text{MoS}_2} = E_{\text{exc}}^{\text{K}} - E_{\text{exc}}^{\text{h}\Sigma} = 0.20 \pm 0.10$ eV with respect to the intralayer K exciton. Hence, accompanied by the emission of a phonon, optically excited K excitons can effectively be transferred to hybrid h Σ excitons. However, the large energy difference $\Delta E_{\text{exc}}^{\text{WSe}_2/\text{MoS}_2}$ strongly suppresses backscattering events for which multiple phonon absorption processes would be required. The

suppression of the backscattering channel in the heterobilayer in comparison to the monolayer is most evident by the much stronger reduction of photoemission intensity from K excitons to below 10% after only 100 fs (green delay-region in figure 5(a)). Photoemission intensity from hybrid $h\Sigma$ excitons, on the other side, rises on the same timescale, which is in agreement with the interpretation of an initially fast transfer of excitons from K to $h\Sigma$ excitons (yellow and green delay-regions in figures 5(b)).

Once the hybrid $h\Sigma$ excitons are formed, they can relax to the ILX by subsequent exciton-phonon scattering processes within the MoS_2 layer. For the analysis of this process, we fit the picosecond evolution of photoemission intensity from hybrid $h\Sigma$ excitons with a biexponential function (figure 5(b)) and extract a fast $h\Sigma \rightarrow \text{ILX}$ decay time of $\tau_{\text{WSe}_2/\text{MoS}_2, \text{fast}}^{h\Sigma} = 110 \pm 40$ fs. Notably, this decay time is in excellent agreement with the rise time of photoemission intensity from ILX (figure 5(b), $\tau_{\text{WSe}_2/\text{MoS}_2, \text{rise}}^{\text{ILX}} = 120 \pm 20$ fs, red data points), being thus a strong indication that ILX excitons are directly formed from hybrid $h\Sigma$ excitons. Again, because of the large energy difference between the hybrid $h\Sigma$ exciton and the ILX, i.e., $\Delta E_{\text{exc}}^{\text{ILX}} = E_{\text{exc}}^{h\Sigma} - E_{\text{exc}}^{\text{ILX}} = 0.26 \pm 0.10$ eV (cf. table I), phonon absorption processes are nearly fully suppressed and backscattering events from ILX to hybrid $h\Sigma$ excitons can also be excluded.

Finally, we note that our experimental observation on the efficiency of forward and backward scattering in the WSe_2 monolayer and the $\text{WSe}_2/\text{MoS}_2$ heterobilayer are fully consistent with our microscopic model. Specifically, for the WSe_2 monolayer, the calculations reproduce the establishment of a steady state $\text{K} \rightleftharpoons \Sigma$ (blue arrows in figure 1(e)). Notably, the model here finds that especially the momentum-indirect excitons, where the hole- and the electron-component are momentum-offset in the K_W and K'_W valleys, contribute to the establishment of the steady state, as detailed, e.g., in refs. [15, 21]. In addition, for the $\text{WSe}_2/\text{MoS}_2$ heterobilayer, the microscopic model reproduces the negligible efficiency for backscattering as compared to the forward scattering leading to the formation of ILX (blue arrows in figure 1(f)).

V. CONCLUSION

In a joint experiment-theory effort, we have used femtosecond momentum microscopy and microscopic modelling to characterize the energy landscape of bright and dark excitons and the resulting scattering dynamics in monolayer WSe_2 and heterobilayer $\text{WSe}_2/\text{MoS}_2$. First, we find that interlayer hybridization in $\text{WSe}_2/\text{MoS}_2$ leads to a reduction of the energy of the optically dark

hybrid exciton when compared to monolayer WSe_2 , where the exciton is localized in the layer. Second, in direct comparison to microscopic modelling, we demonstrate that the hybrid $h\Sigma$ and the intralayer Σ excitons are formed via exciton-phonon scattering. And third, we show that the relative efficiency of phonon absorption and emission processes are the dominant parameter for the different exciton dynamics in monolayer WSe_2 and heterobilayer $\text{WSe}_2/\text{MoS}_2$. Specifically, in monolayer WSe_2 , we showed that the occupation of intralayer K and Σ evolves into a steady state, i.e., $K \rightleftharpoons \Sigma$, and the overall exciton occupation decays via radiative processes of the bright K excitons. In contrast, in the $\text{WSe}_2/\text{MoS}_2$ heterobilayer, we found that the energy level alignment of the contributing excitons strongly suppresses phonon-absorption processes and leads to a true exciton cascade $K \rightarrow \Sigma \rightarrow \text{ILX}$ with negligible contributions of backscattering.

VI. ACKNOWLEDGEMENTS

This work was funded by the Deutsche Forschungsgemeinschaft (DFG, German Research Foundation) - 432680300/SFB 1456, project B01, 217133147/SFB 1073, projects B07 and B10, and 223848855/SFB 1083, project B9. A.A. and S.H. acknowledge funding from EP-SRC (EP/T001038/1, EP/P005152/1). A.A. acknowledges financial support by the Saudi Arabian Ministry of Higher Education. E. M. acknowledges support from the European Unions Horizon 2020 research and innovation programme under grant agreement no. 881603 (Graphene Flagship). K.W. and T.T. acknowledge support from the JSPS KAKENHI (Grant Numbers 20H00354, 21H05233 and 23H02052) and World Premier International Research Center Initiative (WPI), MEXT, Japan.

VII. REFERENCES

- [1] Chenhao Jin, Eric Yue Ma, Ouri Karni, Emma C. Regan, Feng Wang, and Tony F. Heinz, “Ultrafast dynamics in van der Waals heterostructures,” *Nature Nanotechnology* **13**, 994–1003 (2018).
- [2] Pasqual Rivera, Hongyi Yu, Kyle L. Seyler, Nathan P. Wilson, Wang Yao, and Xiaodong Xu, “Interlayer valley excitons in heterobilayers of transition metal dichalcogenides,” *Nature Nanotechnology* **13**, 1004–1015 (2018).
- [3] Dante M. Kennes, Martin Claassen, Lede Xian, Antoine Georges, Andrew J. Millis, James Hone, Cory R. Dean, D. N. Basov, Abhay N. Pasupathy, and Angel Rubio, “Moiré heterostructures as a

- condensed-matter quantum simulator,” *Nature Physics* **17**, 155–163 (2021).
- [4] Nathan P. Wilson, Wang Yao, Jie Shan, and Xiaodong Xu, “Excitons and emergent quantum phenomena in stacked 2D semiconductors,” *Nature* **599**, 383–392 (2021).
- [5] Emma C. Regan, Danqing Wang, Eunice Y. Paik, Yongxin Zeng, Long Zhang, Jihang Zhu, Allan H. MacDonald, Hui Deng, and Feng Wang, “Emerging exciton physics in transition metal dichalcogenide heterobilayers,” *Nature Reviews Materials* **7**, 778–795 (2022).
- [6] Raul Perea-Causin, Daniel Erckensten, Jamie M. Fitzgerald, Joshua J. P. Thompson, Roberto Rosati, Samuel Brem, and Ermin Malic, “Exciton optics, dynamics, and transport in atomically thin semiconductors,” *APL Materials* **10**, 100701 (2022).
- [7] Archana Raja, Malte Selig, Gunnar Berghäuser, Jaeun Yu, Heather M. Hill, Albert F. Rigosi, Louis E. Brus, Andreas Knorr, Tony F. Heinz, Ermin Malic, and Alexey Chernikov, “Enhancement of exciton–phonon scattering from monolayer to bilayer WS_2 ,” *Nano Letters* **18**, 6135–6143 (2018).
- [8] Kin Fai Mak, Changgu Lee, James Hone, Jie Shan, and Tony F. Heinz, “Atomically thin MoS_2 : A new direct-gap semiconductor,” *Physical Review Letters* **105**, 136805 (2010).
- [9] Andrea Splendiani, Liang Sun, Yuanbo Zhang, Tianshu Li, Jonghwan Kim, Chi-Yung Chim, Giulia Galli, and Feng Wang, “Emerging photoluminescence in monolayer MoS_2 ,” *Nano Letters* **10**, 1271–1275 (2010).
- [10] Gang Wang, Alexey Chernikov, Mikhail M. Glazov, Tony F. Heinz, Xavier Marie, Thierry Amand, and Bernhard Urbaszek, “Colloquium: Excitons in atomically thin transition metal dichalcogenides,” *Reviews of Modern Physics* **90**, 021001 (2018).
- [11] Alexey Chernikov, Timothy C. Berkelbach, Heather M. Hill, Albert Rigosi, Yilei Li, Ozgur Burak Aslan, David R. Reichman, Mark S. Hybertsen, and Tony F. Heinz, “Exciton binding energy and nonhydrogenic rydberg series in monolayer WS_2 ,” *Physical Review Letters* **113**, 076802 (2014).
- [12] Keliang He, Nardeep Kumar, Liang Zhao, Zefang Wang, Kin Fai Mak, Hui Zhao, and Jie Shan, “Tightly bound excitons in monolayer WSe_2 ,” *Physical Review Letters* **113**, 026803 (2014).
- [13] Ziliang Ye, Ting Cao, Kevin O’Brien, Hanyu Zhu, Xiaobo Yin, Yuan Wang, Steven G. Louie, and Xiang Zhang, “Probing excitonic dark states in single-layer tungsten disulphide,” *Nature* **513**, 214–218 (2014).
- [14] Hongyi Yu, Yong Wang, Qingjun Tong, Xiaodong Xu, and Wang Yao, “Anomalous Light Cones and Valley Optical Selection Rules of Interlayer Excitons in Twisted Heterobilayers,” *Physical Review Letters* **115**, 187002 (2015).

- [15] Samuel Brem, August Ekman, Dominik Christiansen, Florian Katsch, Malte Selig, Cedric Robert, Xavier Marie, Bernhard Urbaszek, Andreas Knorr, and Ermin Malic, “Phonon-assisted photoluminescence from indirect excitons in monolayers of transition-metal dichalcogenides,” *Nano Letters* **20**, 2849–2856 (2020).
- [16] Xiao-Xiao Zhang, Yumeng You, Shu Yang Frank Zhao, and Tony F. Heinz, “Experimental evidence for dark excitons in monolayer WSe₂,” *Physical Review Letters* **115**, 257403 (2015).
- [17] Dominik Christiansen, Malte Selig, Gunnar Berghäuser, Robert Schmidt, Iris Niehues, Robert Schneider, Ashish Arora, Steffen Michaelis de Vasconcellos, Rudolf Bratschitsch, Ermin Malic, and Andreas Knorr, “Phonon sidebands in monolayer transition metal dichalcogenides,” *Physical Review Letters* **119**, 187402 (2017).
- [18] Malte Selig, Gunnar Berghäuser, Archana Raja, Philipp Nagler, Christian Schüller, Tony F. Heinz, Tobias Korn, Alexey Chernikov, Ermin Malic, and Andreas Knorr, “Excitonic linewidth and coherence lifetime in monolayer transition metal dichalcogenides,” *Nature Communications* **7**, 13279 (2016).
- [19] Ermin Malic, Malte Selig, Maja Feierabend, Samuel Brem, Dominik Christiansen, Florian Wendler, Andreas Knorr, and Gunnar Berghäuser, “Dark excitons in transition metal dichalcogenides,” *Physical Review Materials* **2**, 014002 (2018).
- [20] Thorsten Deilmann and Kristian Sommer Thygesen, “Finite-momentum exciton landscape in mono- and bilayer transition metal dichalcogenides,” *2D Materials* **6**, 035003 (2019).
- [21] Malte Selig, Gunnar Berghäuser, Marten Richter, Rudolf Bratschitsch, Andreas Knorr, and Ermin Malic, “Dark and bright exciton formation, thermalization, and photoluminescence in monolayer transition metal dichalcogenides,” *2D Materials* **5**, 035017 (2018).
- [22] Pramoda K. Nayak, Yevhen Horbatenko, Seongjoon Ahn, Gwangwoo Kim, Jae-Ung Lee, Kyung Yeol Ma, A. Rang Jang, Hyunseob Lim, Dogyeong Kim, Sunmin Ryu, Hyeonsik Cheong, Noejung Park, and Hyeon Suk Shin, “Probing evolution of twist-angle-dependent interlayer excitons in MoSe₂/WSe₂ van der waals heterostructures,” *ACS Nano* **11**, 4041–4050 (2017).
- [23] C. Poellmann, P. Steinleitner, U. Leierseder, P. Nagler, G. Plechinger, M. Porer, R. Bratschitsch, C. Schüller, T. Korn, and R. Huber, “Resonant internal quantum transitions and femtosecond radiative decay of excitons in monolayer WSe₂,” *Nature Materials* **14**, 889–893 (2015).
- [24] P. Merkl, F. Mooshammer, P. Steinleitner, A. Girnguber, K. Q. Lin, P. Nagler, J. Holler, C. Schüller, J. M. Lupton, T. Korn, S. Ovesen, S. Brem, E. Malic, and R. Huber, “Ultrafast transition between exciton phases in van der Waals heterostructures,” *Nature Materials* **18**, 691–696 (2019).

- [25] Marius Keunecke, Christina Möller, David Schmitt, Hendrik Nolte, G. S. Matthijs Jansen, Marcel Reutzel, Marie Gutberlet, Gyula Halasi, Daniel Steil, Sabine Steil, and Stefan Mathias, “Time-resolved momentum microscopy with a 1 MHz high-harmonic extreme ultraviolet beamline,” *Review of Scientific Instruments* **91**, 063905 (2020).
- [26] M. Puppin, Y. Deng, C. W. Nicholson, J. Feldl, N. B. M. Schröter, H. Vita, P. S. Kirchmann, C. Monney, L. Rettig, M. Wolf, and R. Ernstorfer, “Time- and angle-resolved photoemission spectroscopy of solids in the extreme ultraviolet at 500 kHz repetition rate,” *Review of Scientific Instruments* **90**, 023104 (2019).
- [27] C. M. Heyl, J. GÜdde, A. L’Huillier, and U. Höfer, “High-order harmonic generation with μJ laser pulses at high repetition rates,” *Journal of Physics B: Atomic, Molecular and Optical Physics* **45**, 074020 (2012).
- [28] Xinlong Li, Melanie A. R. Reber, Christopher Corder, Yuning Chen, Peng Zhao, and Thomas K. Allison, “High-power ultrafast Yb: fiber laser frequency combs using commercially available components and basic fiber tools,” *Review of Scientific Instruments* **87**, 093114 (2016).
- [29] Jonathan A. Sobota, Yu He, and Zhi-Xun Shen, “Angle-resolved photoemission studies of quantum materials,” *Reviews of Modern Physics* **93**, 025006 (2021).
- [30] Uwe Bovensiepen, Hrvoje Petek, and Martin Wolf, *Dynamics at Solid State Surfaces and Interfaces*, 1st ed., Vol. 2: Fundamentals (Wiley-VCH Verlag GmbH & Co., Weinheim, 2012).
- [31] R. Bertoni, C. W Nicholson, L. Waldecker, H. Hübener, C. Monney, U. De Giovannini, M. Puppin, M. Hoesch, E. Springate, R. T Chapman, C. Cacho, M. Wolf, A. Rubio, and R. Ernstorfer, “Generation and evolution of spin-, valley-, and layer-polarized excited carriers in inversion-symmetric WSe_2 ,” *Physical Review Letters* **117**, 277201 (2016).
- [32] R. Wallauer, J. Reimann, N. Armbrust, J. GÜdde, and U. Höfer, “Intervalley scattering in MoS_2 imaged by two-photon photoemission with a high-harmonic probe,” *Applied Physics Letters* **109**, 162102 (2016).
- [33] P. Hein, A. Stange, K. Hanff, L. X. Yang, G. Rohde, K. Rossnagel, and M. Bauer, “Momentum-resolved hot electron dynamics at the 2H-MoS_2 surface,” *Physical Review B* **94**, 205406 (2016).
- [34] R. Wallauer, P. Marauhn, J. Reimann, S. Zoerb, F. Kraus, J. GÜdde, M. Rohlfig, and U. Höfer, “Momentum-resolved observation of ultrafast interlayer charge transfer between the topmost layers of MoS_2 ,” *Physical Review B* **102**, 125417 (2020).

- [35] Shuo Dong, Michele Puppin, Tommaso Pincelli, Samuel Beaulieu, Dominik Christiansen, Hannes Hübener, Christopher W. Nicholson, Rui Patrick Xian, Maciej Dendzik, Yunpei Deng, Yoav William Windsor, Malte Selig, Ermin Malic, Angel Rubio, Andreas Knorr, Martin Wolf, Laurenz Rettig, and Ralph Ernstorfer, “Direct measurement of key exciton properties: Energy, dynamics, and spatial distribution of the wave function,” *Natural Sciences* **1**, e10010 (2021).
- [36] Antonija Grubišić Čabo, Jill A. Miwa, Signe S. Grønberg, Jonathon M. Riley, Jens C. Johannsen, Cephise Cacho, Oliver Alexander, Richard T. Chapman, Emma Springate, Marco Grioni, Jeppe V. Lauritsen, Phil D. C. King, Philip Hofmann, and Søren Ulstrup, “Observation of ultrafast free carrier dynamics in single layer MoS₂,” *Nano Letters* **15**, 5883–5887 (2015).
- [37] Fang Liu, Mark E. Ziffer, Kameron R. Hansen, Jue Wang, and Xiaoyang Zhu, “Direct Determination of Band-Gap Renormalization in the Photoexcited Monolayer MoS₂,” *Physical Review Letters* **122**, 246803 (2019).
- [38] Yi Lin, Yang-hao Chan, Woojoo Lee, Li-Syuan Lu, Zhenglu Li, Wen-Hao Chang, Chih-Kang Shih, Robert A. Kaindl, Steven G. Louie, and Alessandra Lanzara, “Exciton-driven renormalization of quasiparticle band structure in monolayer MoS₂,” *Physical Review B* **106**, L081117 (2022).
- [39] Woojoo Lee, Yi Lin, Li-Syuan Lu, Wei-Chen Chueh, Mengke Liu, Xiaoqin Li, Wen-Hao Chang, Robert A. Kaindl, and Chih-Kang Shih, “Time-resolved ARPES determination of a quasi-particle band gap and hot electron dynamics in monolayer MoS₂,” *Nano Letters* **21**, 7363–7370 (2021).
- [40] Sven Aeschlimann, Antonio Rossi, Mariana Chávez-Cervantes, Razvan Krause, Benito Arnoldi, Benjamin Stadtmüller, Martin Aeschlimann, Stiven Forti, Filippo Fabbri, Camilla Coletti, and Isabella Gierz, “Direct evidence for efficient ultrafast charge separation in epitaxial WS₂/graphene heterostructures,” *Science Advances* **6**, eaay0761 (2020).
- [41] B. Krömker, M. Escher, D. Funnemann, D. Hartung, H. Engelhard, and J. Kirschner, “Development of a momentum microscope for time resolved band structure imaging,” *Rev. Sci. Instrum.* **79**, 053702–7 (2008).
- [42] K. Medjanik, O. Fedchenko, S. Chernov, D. Kutnyakhov, M. Ellguth, A. Oelsner, B. Schönhense, T. R. F. Peixoto, P. Lutz, C.-H. Min, F. Reinert, S. Däster, Y. Acremann, J. Viehhaus, W. Wurth, H. J. Elmers, and G. Schönhense, “Direct 3D mapping of the Fermi surface and Fermi velocity,” *Nature Materials* **16**, 615–621 (2017).
- [43] Julien Madéo, Michael K. L. Man, Chakradhar Sahoo, Marshall Campbell, Vivek Pareek, E. Laine Wong, Abdullah Al-Mahboob, Nicholas S. Chan, Arka Karmakar, Bala Murali Krishna Mariserla,

- Xiaoqin Li, Tony F. Heinz, Ting Cao, and Keshav M. Dani, “Directly visualizing the momentum-forbidden dark excitons and their dynamics in atomically thin semiconductors,” *Science* **370**, 1199–1204 (2020).
- [44] Robert Wallauer, Raul Perea-Causin, Lasse Münster, Sarah Zajusch, Samuel Brem, Jens Gütde, Katsumi Tanimura, Kai-Qiang Lin, Rupert Huber, Ermin Malic, and Ulrich Höfer, “Momentum-resolved observation of exciton formation dynamics in monolayer WS_2 ,” *Nano Letters* **21**, 5867–5873 (2021).
- [45] Alice Kunin, Sergey Chernov, Jin Bakalis, Ziling Li, Shuyu Cheng, Zachary H. Withers, Michael G. White, Gerd Schönense, Xu Du, Roland K. Kawakami, and Thomas K. Allison, “Momentum-resolved exciton coupling and valley polarization dynamics in monolayer WS_2 ,” *Physical Review Letters* **130**, 046202 (2023).
- [46] David Schmitt, Jan Philipp Bange, Wiebke Bennecke, AbdulAziz AlMutairi, Giuseppe Meneghini, Kenji Watanabe, Takashi Taniguchi, Daniel Steil, D. Russell Luke, R. Thomas Weitz, Sabine Steil, G. S. Matthijs Jansen, Samuel Brem, Ermin Malic, Stephan Hofmann, Marcel Reutzel, and Stefan Mathias, “Formation of moiré interlayer excitons in space and time,” *Nature* **608**, 499–503 (2022).
- [47] Jan Philipp Bange, David Schmitt, Wiebke Bennecke, Giuseppe Meneghini, AbdulAziz AlMutairi, Kenji Watanabe, Takashi Taniguchi, Daniel Steil, Sabine Steil, R. Thomas Weitz, G. S. Matthijs Jansen, Stephan Hofmann, Samuel Brem, Ermin Malic, Marcel Reutzel, and Stefan Mathias, “Probing correlations in the exciton landscape of a moiré heterostructure,” *arXiv e-prints*, arXiv:2303.17886 (2023), arXiv:2303.17886 [cond-mat.mtrl-sci].
- [48] Yong Wang, Zhan Wang, Wang Yao, Gui-Bin Liu, and Hongyi Yu, “Interlayer coupling in commensurate and incommensurate bilayer structures of transition-metal dichalcogenides,” *Physical Review B* **95**, 115429 (2017).
- [49] Giuseppe Meneghini, Samuel Brem, and Ermin Malic, “Ultrafast phonon-driven charge transfer in van der Waals heterostructures,” *Natural Sciences* **2**, e20220014 (2022).
- [50] Jonas E. Zimmermann, Marleen Axt, Fabian Mooshammer, Philipp Nagler, Christian Schüller, Tobias Korn, Ulrich Höfer, and Gerson Mette, “Ultrafast charge-transfer dynamics in twisted $\text{MoS}_2/\text{WSe}_2$ heterostructures,” *ACS Nano* **15**, 14725–14731 (2021).
- [51] Jens Kunstmann, Fabian Mooshammer, Philipp Nagler, Andrey Chaves, Frederick Stein, Nicola Paradiso, Gerd Plechinger, Christoph Strunk, Christian Schüller, Gotthard Seifert, David R. Reichman, and Tobias Korn, “Momentum-space indirect interlayer excitons in transition-metal dichalcogenide van der Waals heterostructures,” *Nature Physics* **14**, 801–805 (2018).

- [52] Veronica R. Policht, Henry Mittenzwey, Oleg Dogadov, Manuel Katzer, Andrea Villa, Qiuyang Li, Benjamin Kaiser, Aaron M. Ross, Francesco Scotognella, Xiaoyang Zhu, Andreas Knorr, Malte Selig, Giulio Cerullo, and Stefano Dal Conte, “Time-domain observation of interlayer exciton formation and thermalization in a $\text{MoSe}_2/\text{WSe}_2$ heterostructure,” arXiv e-prints , arXiv:2304.03707 (2023), arXiv:2304.03707 [cond-mat.mtrl-sci].
- [53] Evgeny M. Alexeev, David A. Ruiz-Tijerina, Mark Danovich, Matthew J. Hamer, Daniel J. Terry, Pramoda K. Nayak, Seongjoon Ahn, Sangyeon Pak, Juwon Lee, Jung Inn Sohn, Maciej R. Molas, Maciej Koperski, Kenji Watanabe, Takashi Taniguchi, Kostya S. Novoselov, Roman V. Gorbachev, Hyeon Suk Shin, Vladimir I. Fal’ko, and Alexander I. Tartakovskii, “Resonantly hybridized excitons in moiré superlattices in van der Waals heterostructures,” *Nature* **567**, 81–86 (2019).
- [54] Kha Tran, Galan Moody, Fengcheng Wu, Xiaobo Lu, Junho Choi, Kyoungwan Kim, Amrithesh Rai, Daniel A. Sanchez, Jiamin Quan, Akshay Singh, Jacob Embley, André Zepeda, Marshall Campbell, Travis Autry, Takashi Taniguchi, Kenji Watanabe, Nanshu Lu, Sanjay K. Banerjee, Kevin L. Silverman, Suenne Kim, Emanuel Tutuc, Li Yang, Allan H. MacDonald, and Xiaoqin Li, “Evidence for moiré excitons in van der Waals heterostructures,” *Nature* **567**, 71–75 (2019).
- [55] Kyle L. Seyler, Pasqual Rivera, Hongyi Yu, Nathan P. Wilson, Essance L. Ray, David G. Mandrus, Jiaqiang Yan, Wang Yao, and Xiaodong Xu, “Signatures of moiré-trapped valley excitons in $\text{MoSe}_2/\text{WSe}_2$ heterobilayers,” *Nature* **567**, 66–70 (2019).
- [56] Chenhao Jin, Emma C. Regan, Aiming Yan, M. Iqbal Bakti Utama, Danqing Wang, Sihan Zhao, Ying Qin, Sijie Yang, Zhiren Zheng, Shenyang Shi, Kenji Watanabe, Takashi Taniguchi, Sefaattin Tongay, Alex Zettl, and Feng Wang, “Observation of moiré excitons in WSe_2/WS_2 heterostructure superlattices,” *Nature* **567**, 76–80 (2019).
- [57] Jessica Lindlau, Malte Selig, Andre Neumann, Léo Colombier, Jonathan Förste, Victor Funk, Michael Förg, Jonghwan Kim, Gunnar Berghäuser, Takashi Taniguchi, Kenji Watanabe, Feng Wang, Ermin Malic, and Alexander Högele, “The role of momentum-dark excitons in the elementary optical response of bilayer WSe_2 ,” *Nature Communications* **9**, 2586 (2018).
- [58] Gunnar Berghäuser, Philipp Steinleitner, Philipp Merkl, Rupert Huber, Andreas Knorr, and Ermin Malic, “Mapping of the dark exciton landscape in transition metal dichalcogenides,” *Physical Review B* **98**, 020301 (2018).
- [59] Fedele Tagarelli, Edoardo Lopriore, Daniel Erkensten, Raül Perea-Causín, Samuel Brem, Joakim Hagel, Zhe Sun, Gabriele Pasquale, Kenji Watanabe, Takashi Taniguchi, Ermin Malic, and Andras

- Kis, “Electrical control of hybrid exciton transport in a van der Waals heterostructure,” *Nature Photonics* (2023), 10.1038/s41566-023-01198-w.
- [60] Samuel Brem, Kai-Qiang Lin, Roland Gillen, Jonas M Bauer, Janina Maultzsch, John M Lupton, and Ermin Malic, “Hybridized intervalley moiré excitons and flat bands in twisted WSe₂ bilayers,” *Nanoscale* **12**, 11088–11094 (2020).
- [61] Samuel Brem, Malte Selig, Gunnar Berghaeuser, and Ermin Malic, “Exciton relaxation cascade in two-dimensional transition metal dichalcogenides,” *Scientific Reports* **8**, 8238 (2018).
- [62] Ouri Karni, Elyse Barré, Sze Cheung Lau, Roland Gillen, Eric Yue Ma, Bumho Kim, Kenji Watanabe, Takashi Taniguchi, Janina Maultzsch, Katayun Barmak, Ralph H. Page, and Tony F. Heinz, “Infrared Interlayer Exciton Emission in MoS₂/WSe₂ Heterostructures,” *Physical Review Letters* **123**, 247402 (2019).
- [63] Haiming Zhu, Jue Wang, Zizhou Gong, Young Duck Kim, James Hone, and X. Y. Zhu, “Interfacial charge transfer circumventing momentum mismatch at two-dimensional van der Waals heterojunctions,” *Nano Letters* **17**, 3591–3598 (2017).
- [64] Yilei Li, Alexey Chernikov, Xian Zhang, Albert Rigosi, Heather M. Hill, Arend M. van der Zande, Daniel A. Chenet, En-Min Shih, James Hone, and Tony F. Heinz, “Measurement of the optical dielectric function of monolayer transition-metal dichalcogenides: MoS₂, MoSe₂, WS₂, and WSe₂,” *Physical Review B* **90**, 205422 (2014).
- [65] T. Taniguchi and K. Watanabe, “Synthesis of high-purity boron nitride single crystals under high pressure by using Ba–BN solvent,” *Journal of Crystal Growth* **303**, 525–529 (2007).
- [66] Søren Ulstrup, Roland J. Koch, Daniel Schwarz, Kathleen M. McCreary, Berend T. Jonker, Simranjeet Singh, Aaron Bostwick, Eli Rotenberg, Chris Jozwiak, and Jyoti Katoch, “Imaging microscopic electronic contrasts at the interface of single-layer WS₂ with oxide and boron nitride substrates,” *Applied Physics Letters* **114**, 151601 (2019).
- [67] Marius Keunecke, Marcel Reutzler, David Schmitt, Alexander Osterkorn, Tridev A. Mishra, Christina Möller, Wiebke Bennecke, G. S. Matthijs Jansen, Daniel Steil, Salvatore R. Manmana, Sabine Steil, Stefan Kehrein, and Stefan Mathias, “Electromagnetic dressing of the electron energy spectrum of Au(111) at high momenta,” *Physical Review B* **102**, 161403 (2020).
- [68] Andi Li, Marcel Reutzler, Zehua Wang, David Schmitt, Marius Keunecke, Wiebke Bennecke, G. S. Matthijs Jansen, Daniel Steil, Sabine Steil, Dino Novko, Branko Gumhalter, Stefan Mathias, and Hrvoje Petek, “Multidimensional multiphoton momentum microscopy of the anisotropic Ag(110) sur-

- face,” *Physical Review B* **105**, 075105 (2022).
- [69] Marten Düvel, Marco Merboldt, Jan Philipp Bange, Hannah Strauch, Michael Stellbrink, Klaus Pierz, Hans Werner Schumacher, Davood Momeni, Daniel Steil, G. S. Matthijs Jansen, Sabine Steil, Dino Novko, Stefan Mathias, and Marcel Reutzler, “Far-from-equilibrium electron–phonon interactions in optically excited graphene,” *Nano Letters* **22**, 4897–4904 (2022).
- [70] G. S. M. Jansen, M. Keunecke, M. Düvel, C. Möller, D. Schmitt, W. Bennecke, F. J. S. Kappert, D. Steil, D. R. Luke, S. Steil, and S. Mathias, “Efficient orbital imaging based on ultrafast momentum microscopy and sparsity-driven phase retrieval,” *New Journal of Physics* **22**, 063012 (2020).
- [71] Neil R. Wilson, Paul V. Nguyen, Kyle Seyler, Pasqual Rivera, Alexander J. Marsden, Zachary P. L. Laker, Gabriel C. Constantinescu, Viktor Kandyba, Alexei Barinov, Nicholas D. M. Hine, Xiaodong Xu, and David H. Cobden, “Determination of band offsets, hybridization, and exciton binding in 2D semiconductor heterostructures,” *Science Advances* **3**, e1601832 (2017).
- [72] Conrad H. Stansbury, M. Iqbal Bakti Utama, Claudia G. Fatuzzo, Emma C. Regan, Danqing Wang, Ziyu Xiang, Mingchao Ding, Kenji Watanabe, Takashi Taniguchi, Mark Blei, Yuxia Shen, Stéphane Lorcy, Aaron Bostwick, Chris Jozwiak, Roland Koch, Sefaattin Tongay, José Avila, Eli Rotenberg, Feng Wang, and Alessandra Lanzara, “Visualizing electron localization of WS₂/WSe₂ moiré superlattices in momentum space,” *Science Advances* **7**, eabf4387 (2021).
- [73] Alfred J. H. Jones, Ryan Muzzio, Sahar Pakdel, Deepnarayan Biswas, Davide Curcio, Nicola Lanatà, Philip Hofmann, Kathleen M. McCreary, Berend T. Jonker, Kenji Watanabe, Takashi Taniguchi, Simranjeet Singh, Roland J. Koch, Chris Jozwiak, Eli Rotenberg, Aaron Bostwick, Jill A. Miwa, Jyoti Katoch, and Søren Ulstrup, “Visualizing band structure hybridization and superlattice effects in twisted MoS₂/WS₂ heterobilayers,” *2D Materials* **9**, 015032 (2021).
- [74] Martin Weinelt, Michael Kutschera, Thomas Fauster, and Michael Rohlfing, “Dynamics of exciton formation at the Si(100) c(4 × 2) surface,” *Phys. Rev. Lett.* **92**, 126801 (2004).
- [75] X. Y. Zhu, “How to draw energy level diagrams in excitonic solar cells,” *The Journal of Physical Chemistry Letters* **5**, 2283–2288 (2014).
- [76] E. Perfetto, D. Sangalli, A. Marini, and G. Stefanucci, “First-principles approach to excitons in time-resolved and angle-resolved photoemission spectra,” *Physical Review B* **94**, 245303 (2016).
- [77] Avinash Rustagi and Alexander F. Kemper, “Photoemission signature of excitons,” *Physical Review B* **97**, 235310 (2018).

- [78] Dominik Christiansen, Malte Selig, Ermin Malic, Ralph Ernstorfer, and Andreas Knorr, “Theory of exciton dynamics in time-resolved ARPES: Intra- and intervalley scattering in two-dimensional semiconductors,” *Physical Review B* **100**, 205401 (2019).
- [79] H. Tanimura, K. Tanimura, and P. H. M. van Loosdrecht, “Dynamics of incoherent exciton formation in Cu₂O: Time- and angle-resolved photoemission spectroscopy,” *Physical Review B* **100**, 115204 (2019).
- [80] Michael K. L. Man, Julien Madéo, Chakradhar Sahoo, Kaichen Xie, Marshall Campbell, Vivek Pareek, Arka Karmakar, E Laine Wong, Abdullah Al-Mahboob, Nicholas S. Chan, David R. Bacon, Xing Zhu, Mohamed M. M. Abdelrasoul, Xiaoqin Li, Tony F. Heinz, Felipe H. da Jornada, Ting Cao, and Keshav M. Dani, “Experimental measurement of the intrinsic excitonic wave function,” *Science Advances* **7**, eabg0192 (2021).
- [81] Wiebke Bennecke, Andreas Windischbacher, David Schmitt, Jan Philipp Bange, Ralf Hemm, Christian S. Kern, Gabriele D’Avino, Xavier Blase, Daniel Steil, Sabine Steil, Martin Aeschlimann, Benjamin Stadtmueller, Marcel Reutzler, Peter Puschnig, G. S. Matthijs Jansen, and Stefan Mathias, “Multiorbital exciton formation in an organic semiconductor,” *arXiv e-prints*, arXiv:2303.13904 (2023), arXiv:2303.13904 [cond-mat.mes-hall].
- [82] Philipp Merkl, Fabian Mooshammer, Samuel Brem, Anna Girnghuber, Kai-Qiang Lin, Leonard Weigl, Marlene Liebich, Chaw-Keong Yong, Roland Gillen, Janina Maultzsch, John M. Lupton, Ermin Malic, and Rupert Huber, “Twist-tailoring coulomb correlations in van der Waals homobilayers,” *Nature Communications* **11**, 2167 (2020).
- [83] Arend M. van der Zande, Jens Kunstmann, Alexey Chernikov, Daniel A. Chenet, YuMeng You, Xiaoxiao Zhang, Pinshane Y. Huang, Timothy C. Berkelbach, Lei Wang, Fan Zhang, Mark S. Hybertsen, David A. Muller, David R. Reichman, Tony F. Heinz, and James C. Hone, “Tailoring the electronic structure in bilayer molybdenum disulfide via interlayer twist,” *Nano Letters* **14**, 3869–3875 (2014).
- [84] Kaihui Liu, Liming Zhang, Ting Cao, Chenhao Jin, Diana Qiu, Qin Zhou, Alex Zettl, Peidong Yang, Steve G. Louie, and Feng Wang, “Evolution of interlayer coupling in twisted molybdenum disulfide bilayers,” *Nature Communications* **5**, 4966 (2014).
- [85] Zhenghe Jin, Xiaodong Li, Jeffrey T. Mullen, and Ki Wook Kim, “Intrinsic transport properties of electrons and holes in monolayer transition-metal dichalcogenides,” *Physical Review B* **90**, 045422 (2014).

- [86] Qiannan Cui, Frank Ceballos, Nardeep Kumar, and Hui Zhao, “Transient absorption microscopy of monolayer and bulk WSe₂,” *ACS Nano* **8**, 2970–2976 (2014).
- [87] Chiara Trovatiello, Florian Katsch, Nicholas J. Borys, Malte Selig, Kaiyuan Yao, Rocio Borrego-Varillas, Francesco Scotognella, Ilka Kriegel, Aiming Yan, Alex Zettl, P. James Schuck, Andreas Knorr, Giulio Cerullo, and Stefano Dal Conte, “The ultrafast onset of exciton formation in 2d semiconductors,” *Nature Communications* **11**, 5277 (2020).
- [88] Long Yuan, Biyuan Zheng, Jens Kunstmann, Thomas Brumme, Agnieszka Beata Kuc, Chao Ma, Shibin Deng, Daria Blach, Anlian Pan, and Libai Huang, “Twist-angle-dependent interlayer exciton diffusion in WS₂–WSe₂ heterobilayers,” *Nature Materials* **19**, 617–623 (2020)